Results of the IMO Video Meteor Network – First Quarter 2020

Sirko Molau. Abenstalstr. 13b. 84072 Seysdorf *2023/06/04*

In the first quarter of 2020, little more than 80 video cameras were in operation in the IMO network. The weather was not particularly good as typical for this time of year, but still we could collect a considerable data set of meteor activity in winter (figure 1).

In January, we recorded nearly 38,000 meteors in over 12,000 observing hours. That is 150 hours and 4,000 meteors more than in 2017, which was the best January so far. With nearly 10,000 observing hours and 21,000 meteors, the outcome of February was well below the previous year, but still one of the best February outputs in the history of the IMO network. The same holds for March, where we recorded over 22,000 meteors in more than 11,700 observing hours. In total, the first quarter of 2019 and 2020 delivered nearly the same result, with 2020 being marginal 200 observing hours and 100 meteors ahead.

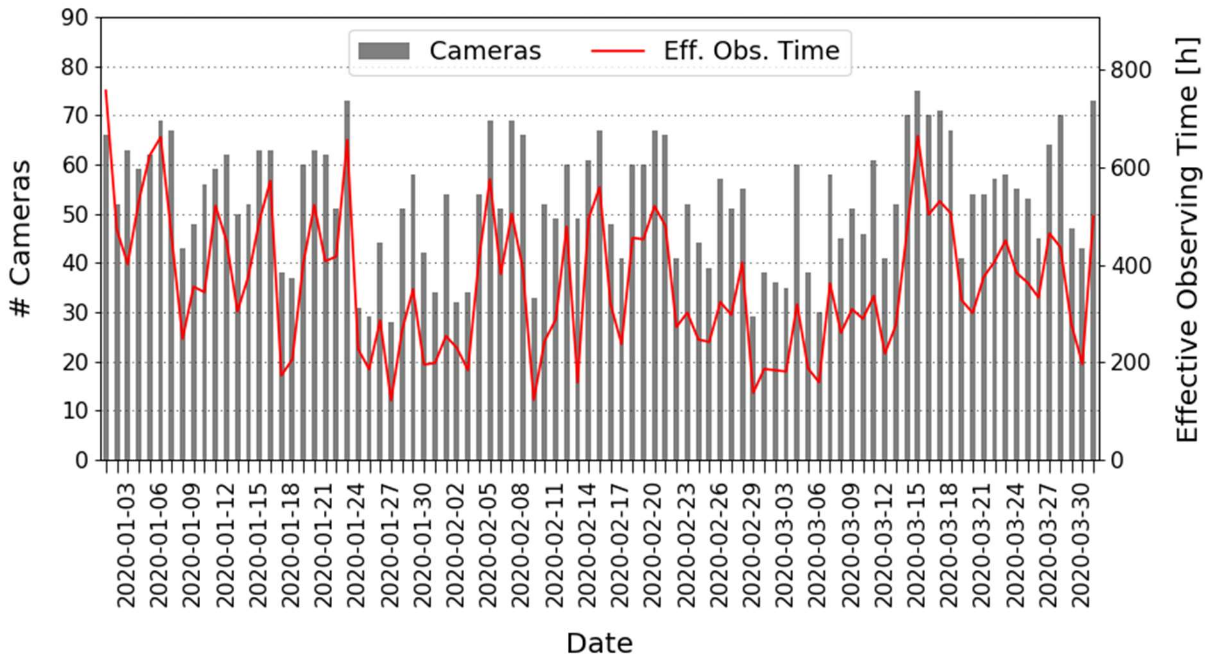

Figure 1: *Number of active cameras per night (grey bars) and effective observing time of these cameras (red line) in the first quarter of 2020.*

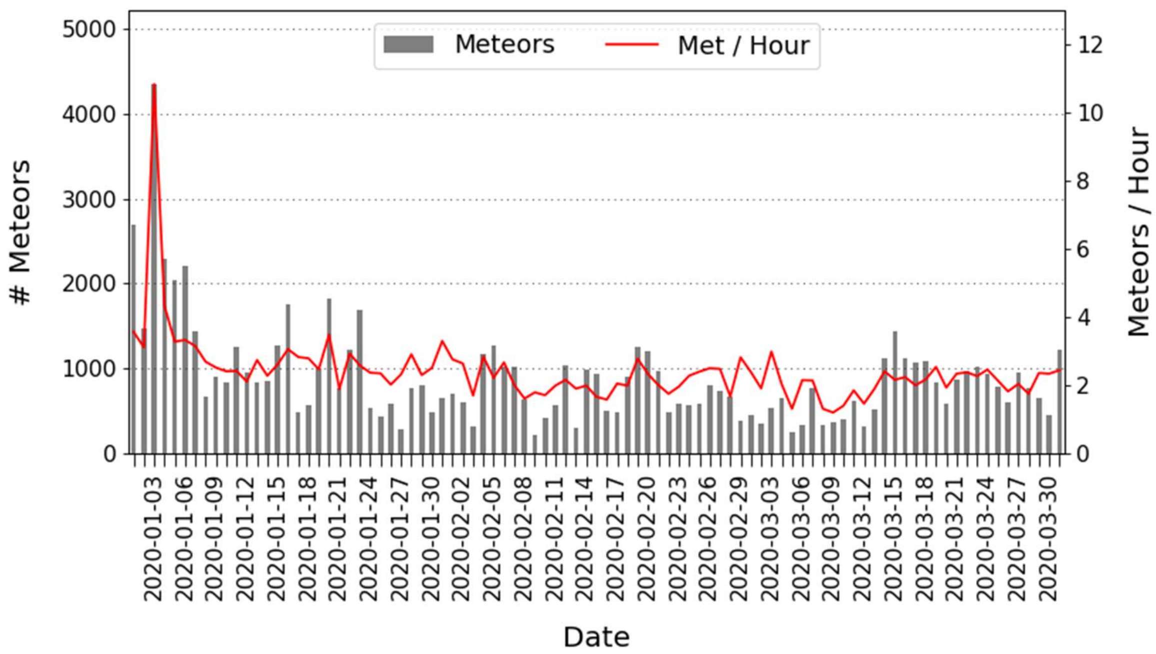

Figure 2: *Number of recorded meteors per night (grey bars) and average number of meteors per hours (red line) in the first quarter of 2020.*

Whereas the hourly meteor count raised shortly during the Quadrantids, it declined thereafter noticeably and reached the annual low of about two meteors per hours in March (figure 2).

Which brings us directly to the only highlight of the review period. The radiant of the Quadrantids raises only after local midnight to substantial heights, so that the waxing moon did not disturb in the relevant second half of night. The peak, however, was predicted for 8 UT on January 4, well beyond the European observing window. Hence, the hourly rates were expected to increase steeply in the morning hours of January 4, when both the shower activity and the radiant altitude were raising. On the other hand, the show should have been over on the next evening, when the steeply falling rates would coincide with a radiant at lower culmination. And that was what we observed. Whereas in the first hour after midnight of January 3/4 we recorded about 100 Quadrantids, it was 700 in the last hour before dawn. On the next evening, the rate had declined to about 10 Quadrantids per hour.
If the meteor counts are corrected for the radiant altitude and other relevant parameters, we obtain a nearly constant flux density of about 20 meteoroids per 1,000 km^2 and hour for the morning of January 4, with even a decreasing tendency towards dawn (figure 3). This implies that the Quadrantid peak 2020 must have been a few hours early.

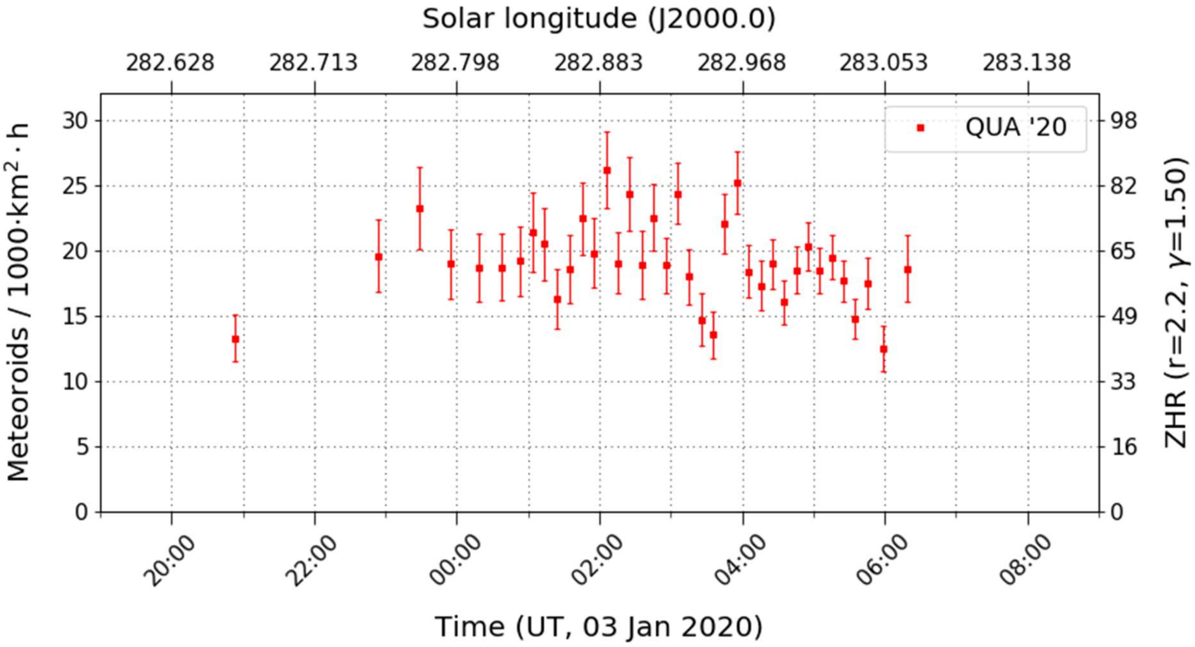

Figure 3: *Flux density of the Quadrantids on January 3/4, 2020, derived from observations of the IMO Network.*

The population index was near r=1.8 in the whole night (figure 4).

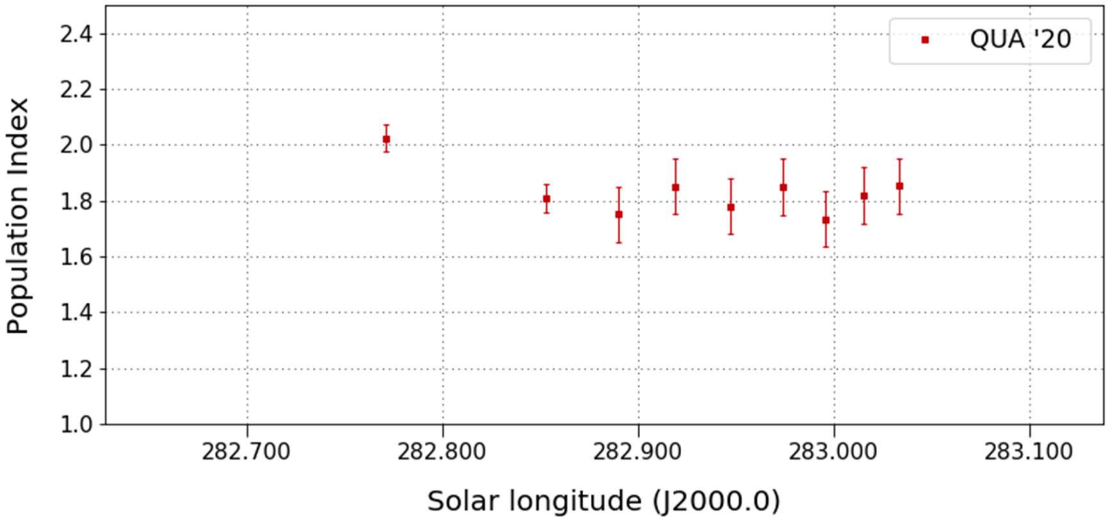

Figure 4: *Population index of the Quadrantids in January 2020.*

The early maximum is confirmed, if we compare the activity profile of 2020 with the long-term average of the years 2011 to 2019 (figure 5, left). It becomes even more obvious, if we add the so far incomplete data sets of 2021 to 2023 (figure 5, right). It seems that starting from 2020 the Quadrantid peak has suddenly shifted backward by 0.4° solar longitude resp.10 hours in time. The visual observations of IMO yield a Quandrantid peak in 2020 at 4 UT, i.e., also earlier than predicted, but not that much.

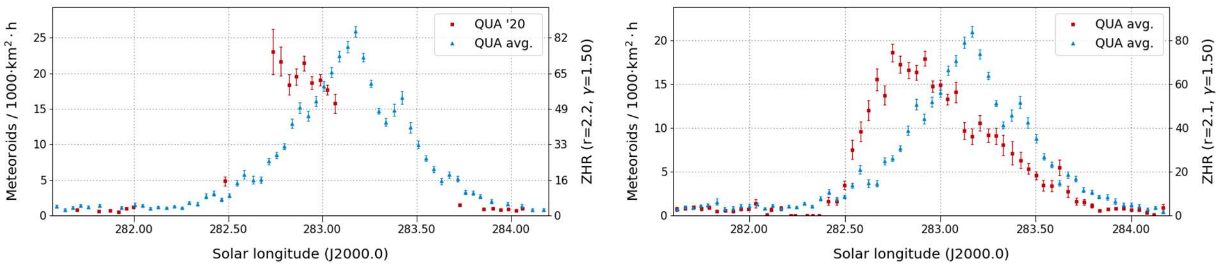

Figure 5: *Comparison of the activity profile of the Quadrantids 2020 with the average of the years 2011 and 2019 (left). On the right side, the 2020 profile was augmented with the already available data of 2021 to 2023.*

And that was about it with meteor shower activity in the first quarter of 2020. Neither the delta Leonids nor any other shower was clearly visible in our data. The flux density of the Antihelion source was less than 1.5 meteoroids per 1,000 km^2 and hour in January and February, and reached values above 1.5 in March (figure 6). The peaks correlate "expectedly" with the times of full moon, which occurred the first decade of each month.

On the IMC 2022 a method to reduce the impact of moon was presented. The flux database was enriched by the sun and moon altitude, the moon phase and the moon distance from the field of view. If observations with significant moon disturbance (moon phase >10%, moon altitude >0°, and moon distance <90°) are left out, the periodic variations get somewhat smaller (figure 7). The result is still not satisfactory, because a noticeable part of observations is omitted and the error bars are getting correspondingly larger.

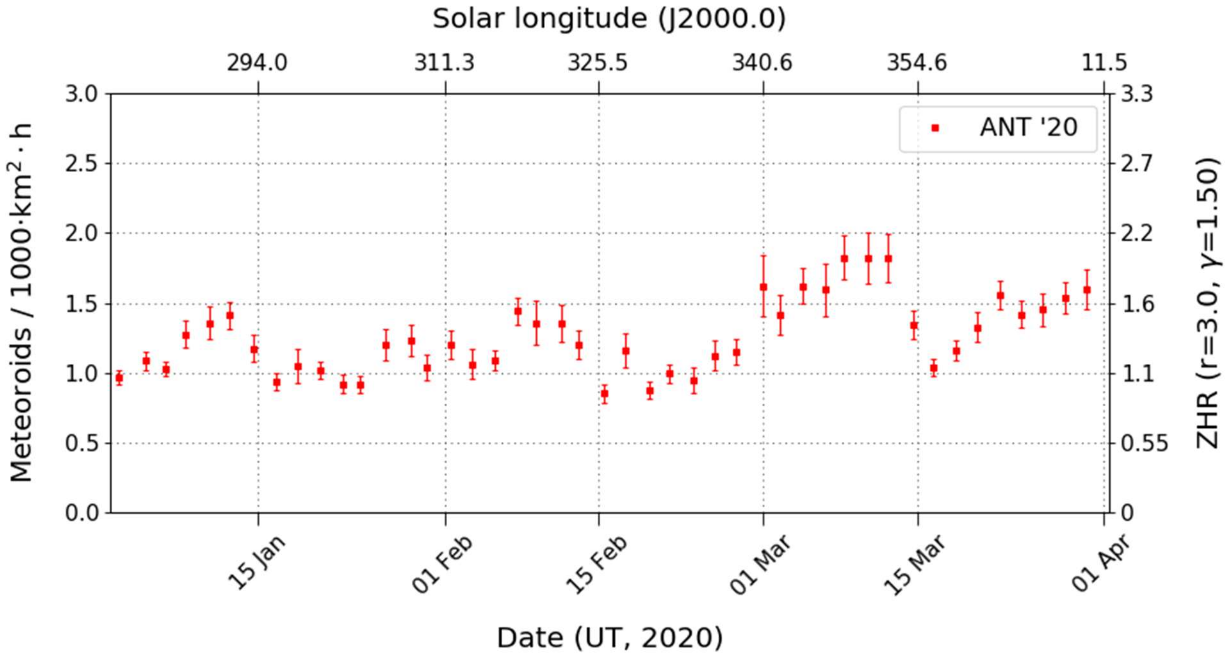

Figure 6: *Activity profile of the Antihelion source in the first quarter of 2020, derived from observations of the IMO Network.*

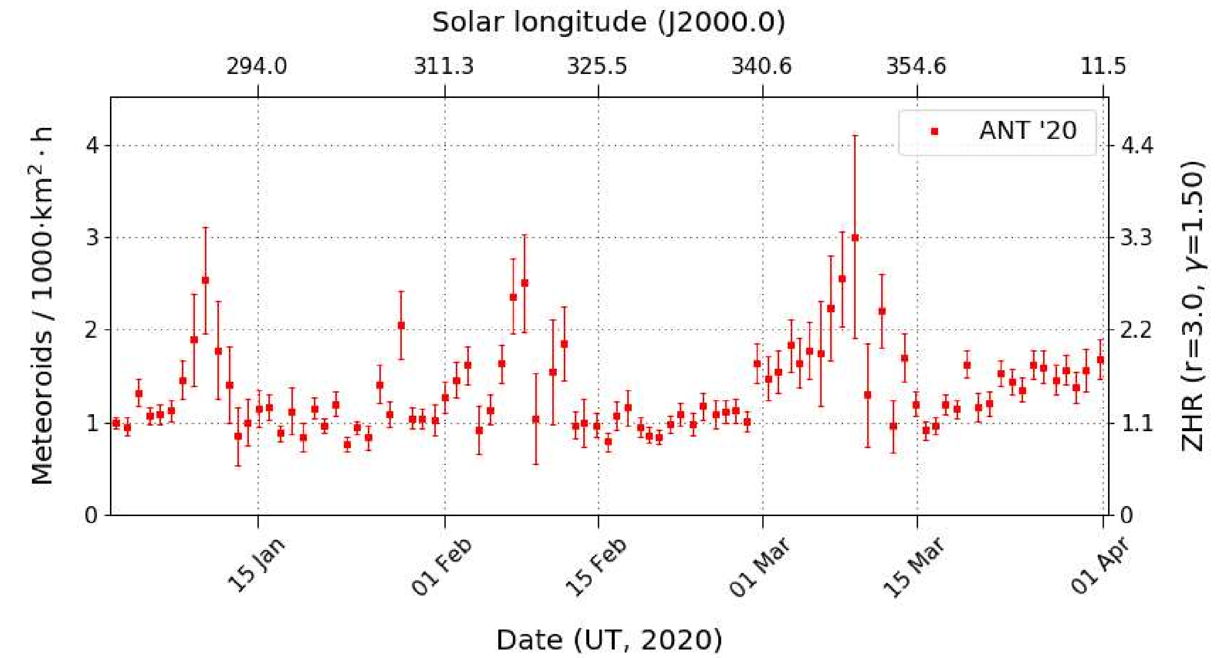

Figure 7: *Activity profile of the Antihelion source in the first quarter of 2020, whereby observations with significant moon disturbance were omitted.*

It would be better, if we could correct the flux density by the moon influence. The relevant parameters are available now – it just needs the right correction function. In the following we will describe how to derive such a correction function.

At first, we need a reliable "calibration standard", i.e., a shower with constant activity and long activity interval. The Antihelion source is the first choice, but is its activity really constant over the year? To determine that, we computed the average Antihelion activity profile from the years 2011 to 2019. In that long time span, the impact of moon should approximately level out. We obtained a profile, that can be approximated by a sum of two sine functions (figure 8).

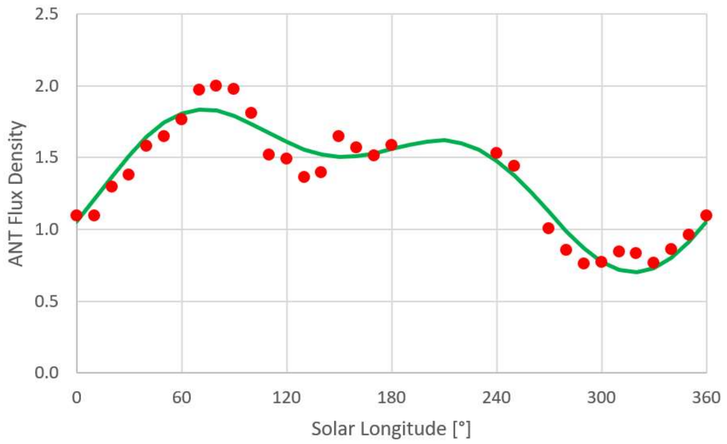

Figure 8: *Average Antihelion activity profile of the years 2011 to 2019, and a fit from the sum of two sine functions.*

The dependency of the flux density FD of the Antihelion source from the solar longitude SL (in degree) can be approximated by:

(1) $$FD = 1.38 + 0.42 \sin(SL - 37) + 0.27 \sin(2xSL - 16)$$

Next, we accumulated all flux density measures of the Antihelion source depending on the corresponding moon parameter, and corrected for the expectation values at the corresponding solar longitude according to eqn. 1. We only used observations where the moon was above the horizon.

In a first test series, we determined the dependency of the Antihelion flux density from the three parameters moon phase, moon altitude and moon distance (from the center of field of view) independently, and fitted a quadratic function with three free parameters each.
Interestingly, the correction for the moon phase was not a monotonic function. The smallest correction was obtained for a moon phase of about 40%. For smaller or larger moon phases, the ANT flux density deviated stronger from the average (figure 9, left). The disadvantage of that modeling is, that the correction remains nearly constant during the night, whereas the impact of the moon on the field of view of the camera is highly variable
For the dependency of the flux density from the moon altitude we got a nearly linear function (figure 9, center). The higher the moon, the larger the correction factor. That is not unexpected, but the moon altitude says little about the brightness or distance of the moon.
The correction factor depends also near linearly from the moon distance (figure 9, right). The farther the moon is away from the field of view, the smaller is the deviation in flux density. The moon brightness is neglected in this case, however.

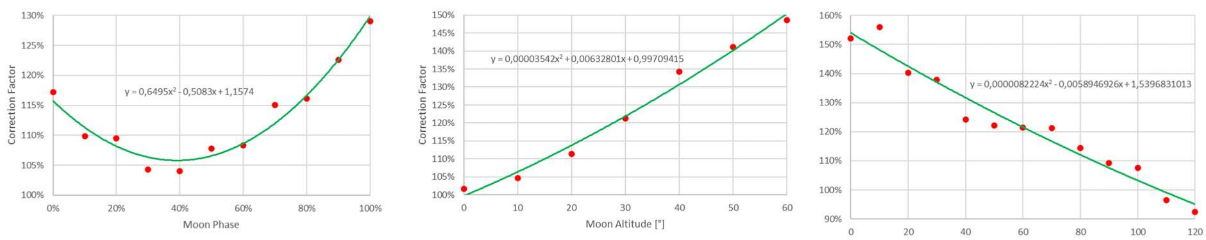

Figure 9: *Impact of the moon phase (left), moon altitude (center) and moon distance from the field of view (right) on the normalized flux density profile of the Antihelion source.*

In figure 10 we show the effect of the quadratic correction functions on the activity profile of the Antihelion source in the first quarter of 2020. The periodic variations are getting smaller in all three cases, but do not disappear completely. All methods perform about equally well, but the moon altitude correction may be subjectively a little better.

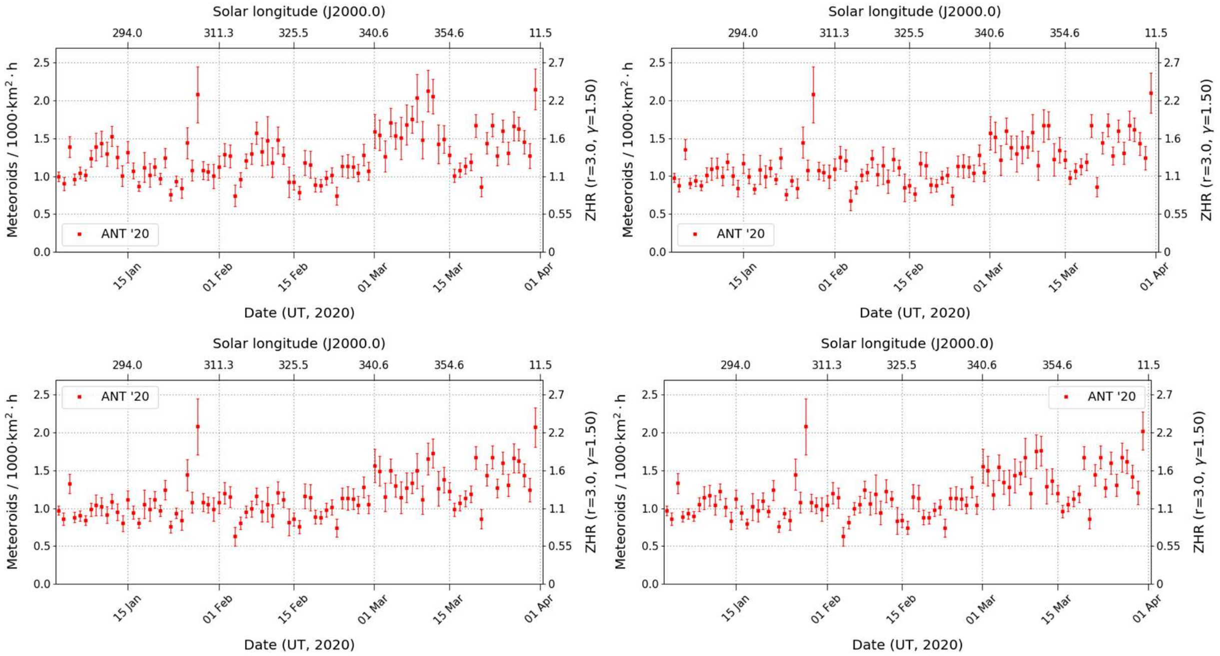

Figure 10: *Uncorrected activity profile of the Antihelion source in the first quarter of 2020 (upper left) and profiles that were corrected for the moon phase (upper right), moon altitude (lower left), and moon distance (lower right).*

Since each parameter alone does not reflect the moon influence completely as described, we started a second test series where we combined two of these three parameters each. The quadratic regression has now nine free parameters and since there are many more parameter combinations, we have fewer observations for each of these. Hence, we see larger scatter in the data. Figure 11 shows in the upper row the original measures and in the lower row the quadratic fit for a combination of the moon phase and altitude (left), moon phase and distance (center) resp. moon altitude and distance (right). It can be seen, that certain parameter combinations cannot occur in the night sky (e.g., a thin crescent near zenith).

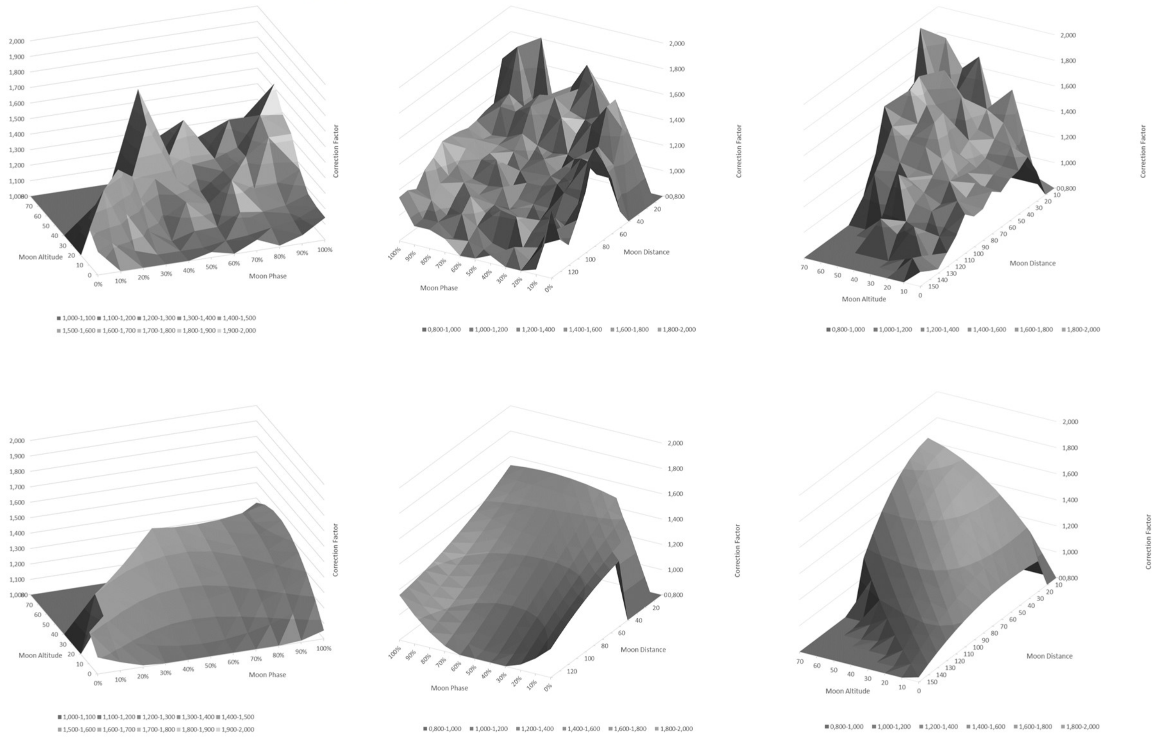

Figure 11: *Impact of the moon phase and altitude (left), moon phase and distance (center) and moon altitude and distance (right) on the normalized flux density profile of the Antihelion source. The upper row shows the original measures, the lower row the quadratic fit.*

Finally, figure 12 shows that the application of these quadratic correction functions further smoothes the activity profile. Again, all the parameter combinations perform equally well, so that there is none which can be particularly recommended. The periodic variations are nearly gone and the expected raise in Antihelion activity toward the end of the first quarter (cf. figure 8) is getting more prominent.

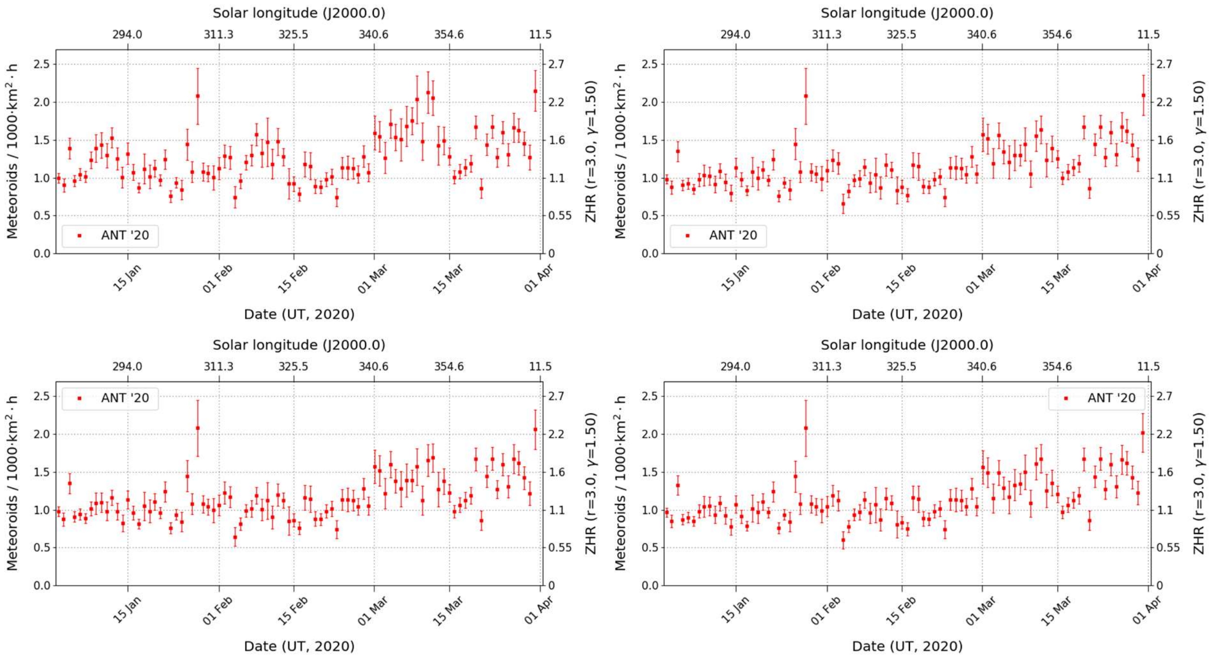

Figure 12: *Uncorrected activity profile of the Antihelion source in the first quarter of 2020 (upper left) and profiles that were corrected for the moon phase and altitude (upper right), moon phase and distance (lower left), and moon altitude and distance (lower right).*

A combination of all three parameters was also tested, but did not yield further improvements. The number of free parameters in the quadratic fit further increases to twenty-seven, and once more there is significantly less data per parameter combination. In addition, this model has more redundancies. The moon altitude is always low for small moon phases, for example, since the moon is setting shortly after the sun resp. rising shortly before it. For the same reason, we see smaller moon distances from the field of view when the moon phase is increasing, and the moon distance is on average smaller for middle moon altitudes, because the cameras are typically not pointed to the horizon or zenith.

All correction options were implemented in MeteorFlux (figure 13), whereby you can select both the parameter combination and the coefficients of the correction function. We will see in the future, if the correction for the moon influence yields the same improvement for other showers than the Antihelion source.

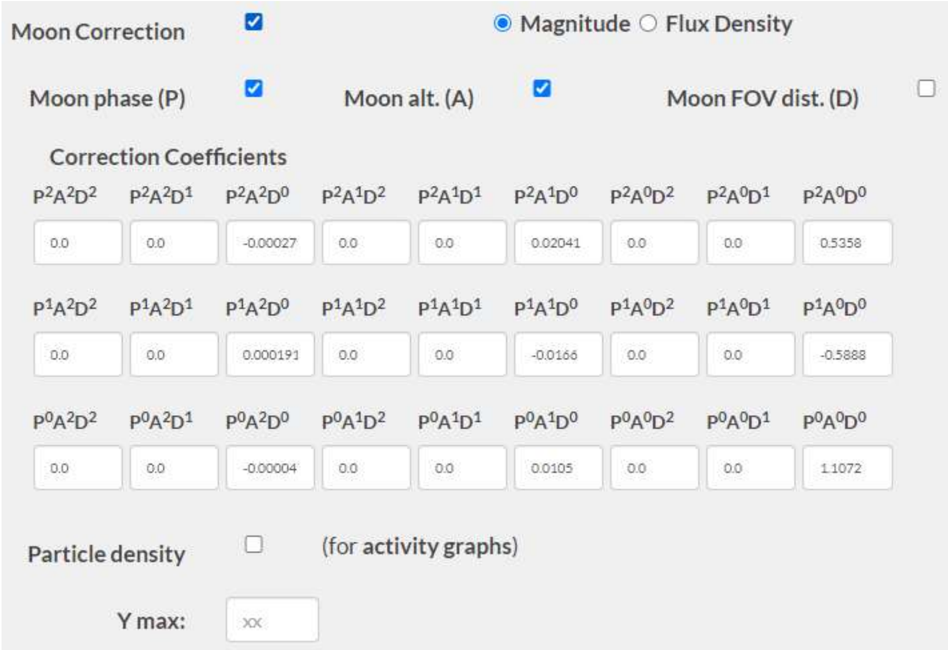

Figure 13: *Implementation of the different correction functions in Meteorflux.*

Table 1: *Observational statistics for first quarter of 2020.*

Code	Name	Place	Camera	January Nights	January Time [h]	January Meteors	February Nights	February Time [h]	February Meteors	March Nights	March Time [h]	March Meteors
ARLRA	Arlt	Ludwigsfelde/DE	LUDWIG2	21	134.9	700	21	86.7	261	27	169.5	646
BERER	Berkó	Ludanyhalaszi/HU	HULUD1	4	38.7	152	-	-	-	-	-	-
BIATO	Bianchi	Mt, San Lorenzo/IT	OMSL1	25	183.7	474	24	201.6	361	22	94.1	169
BOMMA	Bombardini	Faenza/IT	MARIO	26	217.4	691	26	212.9	554	26	170.8	419
BRIBE	Klemt	Herne/DE	HERMINE	19	118.9	288	19	70.4	101	23	147.0	292
		Berg, Gladbach/DE	KLEMOI	21	101.3	241	16	66.2	101	21	141.8	271
CARMA	Carli	Monte Baldo/IT	BMH2	24	274.7	1333	25	258.7	922	20	153.5	534
CASFL	Castellani	Monte Baldo/IT	BMH1	24	261.1	1298	25	262.6	1046	20	151.3	556
CINFR	Cineglosso	Faenza/IT	JENNI	28	225.8	692	26	219.2	611	26	181.9	373
CRIST	Crivello	Valbrevenna/IT	ARCI	23	203.6	621	23	195.1	331	24	138.8	263
			BILBO	23	204.1	897	23	191.5	475	25	163.0	322
			C3P8	20	179.0	407	19	163.5	237	23	162.1	215
			STG38	23	220.9	1060	23	205.5	617	22	169.7	471
ELTMA	Eltri	Venezia/IT	MET38	10	92.9	218	16	139.6	264	19	106.1	180
FORKE	Förster	Carlsfeld/DE	AKM3	15	131.3	374	7	30.0	58	21	161.5	354
GONRU	Goncalves	Tomar/PT	TEMPLAR1	24	156.2	404	26	202.8	462	25	180.0	310
			TEMPLAR2	21	163.4	352	25	204.5	374	24	174.5	259
			TEMPLAR3	16	128.9	112	18	163.7	81	20	146.3	63
			TEMPLAR4	23	141.9	312	23	171.3	274	23	148.8	231
			TEMPLAR5	20	137.4	344	23	176.0	297	22	137.6	157
GOVMI	Govedic	Sredisce ob Dr,/SI	ORION2	23	122.6	409	23	151.7	255	19	134.6	305
			ORION3	22	160.2	206	22	175.1	154	18	117.1	113
			ORION4	20	105.7	179	23	124.6	112	14	63.7	70
HINWO	Hinz	Schwarzenberg/DE	HINWO1	22	174.8	429	16	77.1	133	23	163.8	347
IGAAN	Igaz	Budapest/HU	HUPOL	14	96.7	122	5	23.1	24	13	62.8	59
JONKA	Jonas	Budapest/HU	HUSOR	14	114.1	163	20	131.8	99	19	161.6	110
			HUSOR2	14	118.4	184	21	148.5	137	22	165.5	129
KACJA	Kac	Kamnik/SI	CVETKA	23	199.8	818	14	105.7	285	16	112.9	283
			METKA	23	68.4	167	24	57.0	141	19	41.1	103
			REZIKA	23	209.7	1478	14	98.5	461	16	109.2	508
		Ljubljana/SI	STEFKA	23	216.5	621	14	106.5	176	15	108.7	202
KNOAN	Knöfel	Berlin/DE	ARMEFA	19	132.2	224	14	57.2	69	24	172.8	256
KOSDE	Koschny	La Palma / ES	ICC7	17	96.2	153	16	69.1	83	13	45.8	70
			ICC9	30	255.6	1645	28	218.7	1171	25	168.0	838
			LIC1	11	82.2	123	12	62.6	73	14	45.7	61
			LIC2	29	276	1860	27	216.9	1105	27	185.8	875
KWIMA	Kwinta	Krakow/PL	PAV06	11	91.5	60	9	54.9	30	19	121.6	49
			PAV07	14	118.2	106	8	43.1	34	21	139.7	77
			PAV79	15	127.1	172	11	63.4	78	22	146.2	136
LOJTO	Łojek	Grabniak/PL	PAV103	11	69.8	42	5	33.3	15	7	52.4	28
			PAV57	13	87.8	115	7	53.9	49	9	73.2	85
MACMA	Maciejewski	Chelm/PL	PAV35	16	85.9	122	12	36.7	43	20	120.2	106
			PAV36	17	127.7	169	16	77.5	84	23	165.6	161
			PAV43	16	126.5	219	14	89.9	132	26	173.3	215
			PAV60	17	136.9	241	15	94.3	144	25	179.3	266
MARRU	Marques	Lisbon/PT	CAB1	9	41.2	102	-	-	-	-	-	-
			RAN1	15	130.4	272	19	155.4	160	25	165.4	154
MISST	Missiaggia	Nove/IT	TOALDO	24	233.8	590	1	5.8	3	-	-	-
MOLSI	Molau	Seysdorf/DE	AVIS2	25	160.4	484	22	131.8	357	27	193.8	704
			DIMCAM2	25	154.5	965	23	114.5	607	25	127.6	718
			ESCIMO3	21	164.6	600	21	135.4	435	26	200.9	751
		Ketzür/DE	REMO1	24	123.9	823	25	77.1	295	26	153.9	753
			REMO2	24	151.1	716	23	85.8	239	26	182.8	582
			REMO3	25	177.5	607	25	116.9	238	27	211.8	514
			REMO4	22	163.5	727	24	106.0	277	26	196.0	680
MORJO	Morvai	Fülöpszallas/HU	HUFUL	15	131.8	137	23	167.5	118	21	166.0	95
MOSFA	Moschini	Rovereto/IT	ROVER	29	282.4	541	22	205.8	263	16	103.9	98
NAGHE	Nagy	Budapest/HU	HUKON	-	-	-	23	71.5	183	17	26.2	147
		Piszkestetö/HU	HUPIS	26	140.3	593	25	158.0	250	24	133.1	219
OTTMI	Otte	Pearl City/US	ORIE1	9	4.7	28	14	8.8	40	14	9.1	34
PERZS	Perkó	Becsehely/HU	HUBEC	16	112.1	416	12	88.9	174	8	62.3	91
SARAN	Saraiva	Carnaxide/PT	RO1	25	225.7	384	24	238.9	278	26	213.9	196
			RO2	24	163.8	411	26	226.5	361	27	180.2	232
			RO3	23	174.2	408	25	231.1	446	27	191.7	306
			RO4	24	170.0	290	24	213.9	270	19	120.3	105
SCALE	Scarpa	Alberoni/IT	LEO	22	52.1	216	16	12.3	79	21	10.2	63
SCHHA	Schremmer	Niederkrüchten/DE	DORAEMON	18	89.2	205	22	80.6	128	25	153.0	235
SLAST	Slavec	Ljubljana/SI	KAYAK1	23	183.6	400	13	118.4	184	18	129.6	188
			KAYAK2	24	192.3	158	16	136.2	77	17	143.1	83
STOEN	Stomeo	Scorze/IT	MIN38	28	225.2	1045	22	165.4	553	27	133.6	370
			NOA38	26	228.5	888	21	177.4	478	25	140.4	357
			SCO38	26	244.8	977	22	178.4	563	25	148.8	392
STRJO	Strunk	Herford/DE	BEMCE	19	124.4	860	25	83.9	329	22	151.8	949
			BEMCE2	-	-	-	-	-	-	3	25.1	103
			MINCAM2	17	77.4	174	21	65.0	88	19	102.0	163
			MINCAM3	12	45.6	47	14	49.9	32	21	123.0	246
			MINCAM4	19	112.5	297	19	59.2	79	12	71.0	112
			MINCAM5	19	107.4	192	16	56.6	62	17	131.3	116
TEPIS	Tepliczky	Agostyan/HU	HUAGO	9	59.5	108	2	16.8	47	-	-	-
			HUMOB	17	140.9	453	15	112.4	172	20	150.4	219
WEGWA	Wegrzyk	Nieznaszyn/PL	PAV78	22	127.3	209	14	68.3	48	21	149.3	119
YRJIL	Yrjölä	Kuusankoski/FI	FINEXCAM	14	109.4	337	11	93.2	147	15	94.9	117
ZAKJU	Zakrajšek	Petkovec/SI	PETKA	25	214.1	952	22	176.4	567	22	155.2	492
			TACKA	23	215.2	322	20	177.4	179	19	163.1	162
Sum				**31**	**12171.9**	**37931**	**29**	**9960.3**	**21320**	**31**	**10743.6**	**22401**